Multi-Knowledge Electronic Comprehensive Journal For Education And Science Publications (MECSJ)
ISSUE (28), January (2020)
ISSN: 2616-9185

www.mecsj.com

MICROSTRUCTURE AND NORMAL STATE PROPERTIES FOR YBCO SYSTEM ADDED BY $Zn_{0.95}Fe_{0.05}O$ NANOPARTICLES

[*1]M. Annabi
Umm Al-Qura University, Common First Year Deanship, Makkah, Saudi Arabia
(PB715, Makkah 21955, Saudi Arabia)
[*1]mmannabi@uqu.edu.sa

[2]O. Zayed, [3]M. Fteiti and [4]M. Aouissi
Umm Al-Qura University, Common First Year Deanship, Makkah, Saudi Arabia
(PB715, Makkah 21955, Saudi Arabia)
[2]odzayed@uqu.edu.sa
[3]mafteiti@uqu.edu.sa
[4]mmaouissi@uqu.edu.sa

Abstract

Polycrystalline $YBa_2Cu_3O_y$ (YBCO) samples were synthesized by adding nanoparticles $Zn_{0.95}Fe_{0.05}O$ (ZnFeO) (30 nm in diameter) up to 7 $wt.\%$. By using X-ray diffraction (XRD), no orthorhombic-to-tetragonal phase transition detected up to 5 $wt.\%$ of ZnFeO and lattice parameters remain almost constant. We may conclude that the nano ZnFeO particles are well dispersed at the grain boundaries of the Y-123 matrix. TEM and EDS analyses show the presence of inhomogeneities embedded in the superconducting matrix. These defects can contribute to the scattering of the conduction electrons and increases the residual resistivity with ZnFeO addition. In fact, we note a slowly variation of residual resistivity $\Delta\rho_0$ for $x \leq 1$ then increases more rapidly as the amount of ZnFeO increases. Electrical resistivity measurements show a suppression of the superconductivity at the rate of 8.3K/at% for ZnFeO addition greater than1 $wt.\%$.

A nonmetallic upturn in normal state is observed for ZnFeO addition more than1 $wt.\%$, hence, the temperature dependence electrical resistivity was discussed according to Mott variable range hopping (VRH). It is found that the normal state is governed by two and three variable range hopping (2D-VRH and 3D-VRH) conduction for ZnFeO addition $x \geq 1$ and Coulomb gap (CG) mechanism for$x \leq 0.5$.

The modification of the electrical behavior of YBCO added samples from Coulomb gap to hopping conduction lead to influence the localization length behavior. This result can be interpreted by disorder effect induced by the introduction of nano-size ZnFeO in the matrix.

Key words: A. YBCO; B. Nanometer $Zn_{0.95}Fe_{0.05}O$; C. Structure; D. Electrical properties.

الملخص

تم تحضير عينات (YBCO) $YBa_2Cu_3O_y$ المتعددة البلورات عن طريق إضافة جسيمات نانوية $Zn_{0.95}Fe_{0.05}O$ (ZnFeO) (30 نانومتر في القطر) و بنسب وزنية تصل إلى $7\ wt.\%$. من خلال فحص العينات باستخدام جهاز حيود الأشعة السينية (XRD)، لم تظهر أي انتقالات طورية من orthorhombic (تركيب معيني متعامد) إلى tetragonal (تركيب رباعي الزوايا) لغاية تركيز وزني قدرة $5\ wt.\%$ من ZnFeO , كما بقيت معاملات الشبكة البلورية ثابتة تقريبا.

يقودنا هذا الى استنتاج أن جسيمات ZnFeO النانومترية قد تشتت على حدود الحبيبات المكونة للمركب Y-123. تظهر تحليلات TEM وEDS وجود شوائب متأصلة في المركب الفائق التوصيل. و هذا من شأنه أن يساهم في زيادة تشتت الإلكترونات الموصلة وبالتالي يزيد من المقاومية المتبقية $\Delta\rho_0$ مع إضافة ZnFeO للعينات .

فى الواقع نلاحظ وجود تغير طفيف وبطيء في قيم المقاومية المتبقية $\Delta\rho_0$ عندما تكون $x \leq 1$, ومع زيادة كمية ZnFeO. تزداد المقاومية الكهربائية بشكل سريع .تظهر قياسات المقاومية الكهربائية انحدار الموصلية الفائقة بمعدل 8.3K/at% في حال كانت النسبة الوزنية الضافة ل ZnFeO أكثر من $1\ wt.\%$. و عند إضافة ZnFeO بتراكيز أكثر من $1\ wt.\%$, لوحظ وجود ارتفاع لا فلزي (nonmetallic upturn) في الحالة العادية ، لذلك تمت مناقشة ارتباط المقاومة الكهربائية بدرجة الحرارة وفقا ل (Mott variable range hopping (VRH). ووجد أن الحالة العادية يحكمها آلية التوصيل ثنائي الابعاد او ثلاثي الابعاد وفقا لتركيزZnFeO .(اذا كان تركيز ZnFeO اكبر من او يساوي 1) , بينما استخدمت آلية فجوة Coulomb (CG) لتراكيز اقل من او يساوي 0.5. ان تغير السلوك الكهربائي لعينات YBCO من فجوة Coulomb إلى التوصيل بالقفز اثر على سلوك التموضع الطولي. ويمكن تفسير هذه النتيجة من خلال تأثير التشتت و عدم الترتيب الناجم عن إضافة الجسيمات النانومترية ZnFeO للمركب.

الكلمات المفتاحية : YBCO ، $Zn_{0.95}Fe_{0.05}O$ ، نانومتر، البناء، الخصائص الكهربائية.

1. Introduction

Since their discovery, high-temperature superconductors (HTSC) have not revealed all their secrets despite the extensive research that have been conducted. To better understand the behavior of superconducting materials, a special interest of studies has been reported on the effect of doping as an effective tool to probe the superconducting properties of $YBa_2Cu_3O_y$ (YBCO, or Y-123) compound. The superconducting transition temperatureT_c, normal state, residual resistivity, structure of the YBCO can be modified either by the substitution of elements, by additives or by oxygen disorder [1–15].

Probably Zn impurity is the most widely investigated in d-wave superconductors. It is reported that the superconductivity is suppressed in Zn substituted (Y,Ca)-123 due to pair-breaking processes [16, 17] and the reduction in the critical temperature T_c is about 8-12 K/at% for divalent dopant Zn [18–20]. The dependence between superconducting transition temperature T_c reduction and superfluid density decrease has been reported. In fact, to explain the observed decrease in the muon spin relaxation rate and therefore suppress of superconducting condensate n_s in the presence of Zn impurity in Y-123, Swiss chess model was proposed [21]. Within the framework of this model, the charge carrier in a given area around each Zn impurity are assumed to be excluded from the superconductivity. Impurity can also affect spin fluctuations [22] and induces carrier's localization by disorder in YBCO doped system [9, 23-25]. Pinglin Li et al. [12] reported that Zn ions in Y-123 make a change in the electron structure, resulting in the carrier localization. As a result, it interferes the pairing and transportation of superconducting carriers and then suppresses the superconductivity with the formation of Zn clusters. There is general consensus in the literature that Zn prefers the Cu (2) plane sites without alteration of the orthorhombic symmetry of the YBCO crystal [12, 26]. In the other hand, it has been suggested that the substitution at Cu (2) sites by Zn results in the formation of local magnetic moments at the four nearest neighbor of Cu (2) sites surrounding the Zn impurity [26, 27].

Fe doping in the YBCO superconductor has taken place in the literature. The preferential sites for Fe atoms are at Cu (1) sites in CuO layer predicted in experiments [28] and the material evolves to tetragonal symmetry for the Fe-doped compounds [29]. It is reported that Fe substitution is less effective on Tc at comparable Zn concentration level [30].

The depression of superconductivity is largely attributable to Cu valence and structure change rather than any magnetic property change [31]. Dual doping with Fe and Zn simultaneously in the YBCO system was explored [32]. It's reported that significant higher T_c suppression as compared to separate equivalent doping of either of these impurities. In fact, strains introduced by the two dopants disturbs the charge balance in the coupled chain and plane system and reduce the concentration of mobile holes in the CuO_2 planes as well as the suppression of the order parameter between the CuO_2 planes by the Fe atoms.

Moreover, among the theoretical models of electronic conduction, the variable rang hopping (VRH) between localized states was used for describing the behavior of normal state of HTSC [24]. A crossover from Efros-Shklovskii (ES) to Mott variable rang hopping transport was observed in substituted superconducting materials [24, 33, 34].

Nano-sized particles added in polycrystalline superconductors have generated great interest because they represent an easily controlled and efficient tool for improving the superconducting properties by introducing pinning centers in the matrix [13, 35-39]. nano-sized ZnO additions in bulk Y-123 show significant pinning enhancement [40]. In our knowledge, a few studies have reported on nanoparticles effect on normal state in YBCO system [41, 42].

In the present work, we present an investigation on the $Zn_{0.95}Fe_{0.05}O$ nano-sized particles (30 nm in diameter) additions in YBCO bulk and their influence on the transport properties. For this purpose, a series of YBCO specimens with different amounts of $Zn_{0.95}Fe_{0.05}O$ (0 –7 wt. %) were grown in air by the solid-state reaction. We focus on the analysis of the structure, microstructure and the electrical properties. Then, for the electrical resistivity analyses we applied the quantum percolation theory based on localized states to the normal state resistivity of these samples. This allows us to interpret the linear behavior of resistivity as a function of temperature for the metallic samples with a Coulomb gap (CG) regime and the semiconducting behavior as a function of temperature for the insulating samples using the variable range hopping (VRH) regime.

2. Experimental

The pure and nanometer $Zn_{0.95}Fe_{0.05}O$ (ZnFeO) added YBCO samples were prepared by the conventional solid-state reaction method under identical conditions. The single phase YBCO was synthesized by thoroughly mixing high purity Y_2O_3 (99.9%), Ba_2CO_3 (99.9%) and CuO (99.9%) according to the chemical formula of Y: Ba:Cu = 1:2:3. This mixture of powders was pelletized and then calcined at 950°C for 12 hrs in air with one intermediate grinding. X-ray diffraction confirmed the YBCO structure. During the final processing stage, ZnFeO particles with an average 30 nm in diameter were added separately to the precursor powder YBCO by mixing and hand grinding both powders in an agate mortar. The additional amount, $x\ wt.\%$, of ZnFeO in this case varied from $0.0\ wt.\%$ to $7.0\ wt.\%$ of the total mass of the sample. The non-added powder ($0.0\ wt.\%$) was basically the precursor but hand ground as the others to ensure identical physical conditions for all samples. The mixed powders were pressed into pellets 0.3 mm thick and 5 mm in diameter, under a uniaxial pressure of 900 MPa then sintered at 950°C for 8 hrs in air, thereafter cooled to room temperature at a rate of 4° C/min.

The structure and phase purity were examined by powder XRD using a Philips 1710 diffractometer with CuK_α radiation. The microstructure of samples was characterized using a transmission electron microscope (TEM) (FEI Tecnai G2) operating at 200 kV with a LaB_6 filament. Local chemical analysis was performed using the energy dispersive X-ray spectroscopy (EDS) system attached to the TEM. The resistivity versus temperature variations were measured using the standard four probe technique in a CCS 450 cryostat system. Electrical contacts were made using silver paint and the contact resistance value was approximately 0.5 Ω. The pellets were carefully cut into bars shaped samples with active cross sections for current flow of 0.3 mm^2.

Multi-Knowledge Electronic Comprehensive Journal For Education And Science Publications (MECSJ)
ISSUE (28), January (2020)
ISSN: 2616-9185
www.mecsj.com

3. Results and discussion

The XRD patterns for some typical samples are shown in Fig.1. Characteristic peaks corresponding to different phases are marked on different patterns. The analysis of the data indicates a single-phase perovskite structure YBCO with orthorhombic Pmmm symmetry and small quantities of secondary phases, such as $BaCuO_2$. A very small fraction of impurities for samples with $x = 5$ of ZnFeO are also detected. There was no orthorhombic-to-tetragonal phase transition detected up to $x = 5$ under the accuracy of XRD patterns.

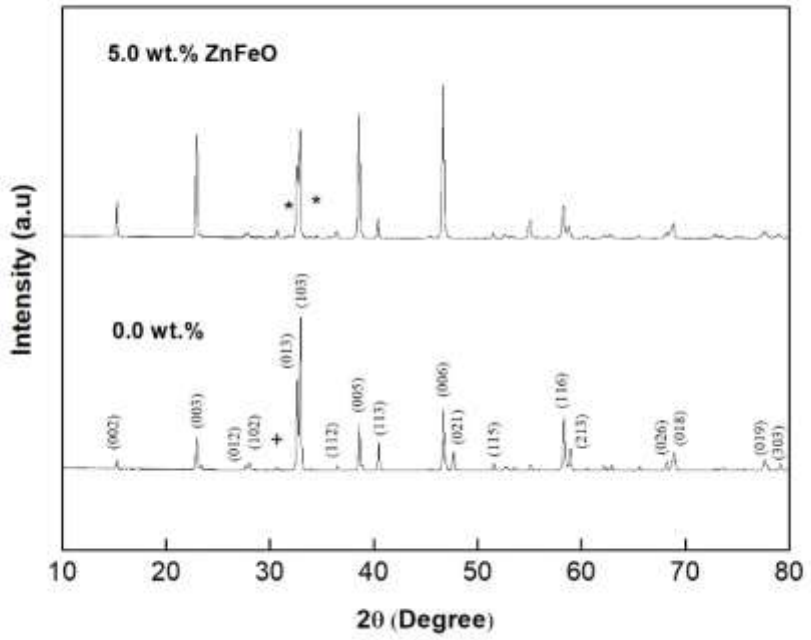

Fig. 1: X-ray powder diffraction patterns of non-added sample and with 5 $wt.\%$ of ZnFeO nanoparticles.
+: $BaCuO_2$ and *: impurity.

The XRD patterns were analyzed by the Rietveld structure refinement method. The structural parameters for the samples were refined so that the calculated pattern fits the observed spectrum very well. The R_p and R_{wp} factors and the goodness of fitting χ^2, were used as the numerical criteria of fitting. Fig. 2a and b show an example of observed and fitted profiles for samples with $x = 0.0$ and $x = 5$ of ZnFeO. It may notice that a, b and c lattice parameters remain almost constant with both additions.

Multi-Knowledge Electronic Comprehensive Journal For Education And Science Publications (MECSJ)
ISSUE (28), January (2020)
ISSN: 2616-9185
www.mecsj.com

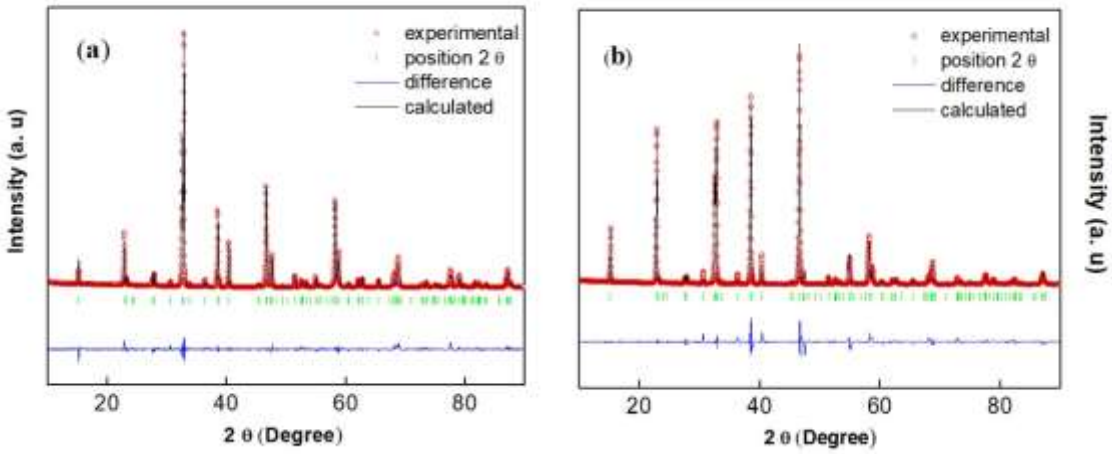

Fig. 2: Rietveld refinement profiles of YBCO samples with: (a) non added and (b) 5 $wt.\%$

ZnFeO addition. The dots are the measured X-ray diffraction data, and the solid line is the calculated profile. The difference curve (observed results minus calculated ones) is plotted at the bottom. The tick marks below represent the positions of Bragg reflections.

The measured lattice parameters are $a = 0.382\ nm$, $b = 0.388\ nm$, $c = 1.168\ nm$ with an estimated 0.0005nm precision. Samples sintered with different addition of nano ZnFeO remained orthorhombic, with the distortion (b–a)/ (a + b) close to that of pristine sample (8.10^{-3}), such value is comparable with the previously reported [43]. In literature, it has been reported by many groups that the crystal structure remained almost unchanged by nanoparticles additions and the different types of nanoparticles occupy the inter-granular spaces in the bulk of different superconducting matrix [35, 44, 45]. We may conclude that the nano ZnFeO particles are well dispersed at the grain boundaries of the Y-123 matrix.

From our lattice parameter c and the relation y = 75.25 - 5.856 c [46], the oxygen content was insignificantly changed and varied from 6.83 for $x = 0.0\ wt.\%$ to 6.80 for $x = 5\ wt.\%$ of ZnFeO. Similar results were reported in the case of nano ZnO addition [41] and Zn-doped Y-123 [29, 47, 48]. In fact, the lattice parameters a, b and c change slightly with the doping of Zn, the oxygen content is independent of Zn doping and all samples are orthorhombic. Hence, any phenomenon that may occur in this study is assumed to be irrelevant to the structure change of these samples.

Multi-Knowledge Electronic Comprehensive Journal For Education And Science Publications (MECSJ)
ISSUE (28), January (2020)
ISSN: 2616-9185
www.mecsj.com

It is known that the sample preparation process and ultimately the microstructure of the resultant material have a direct effect on the transport properties. In order to obtain more detailed information on the microstructure of samples, we performed TEM observations coupled with EDS analyses. Fig. 3a and b illustrate a TEM images for ZnFeO added sample with different orientations of specimen. These figures corresponding to sample sintered with $x = 5\ wt.\%$.

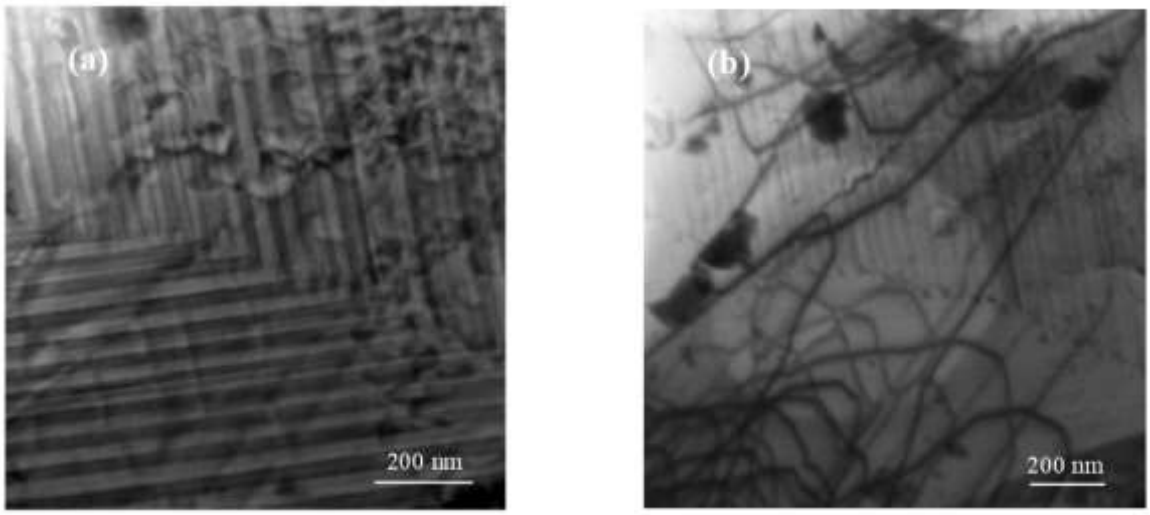

Fig. 3: TEM micrographs of samples sintered with nanosized particles: (a) 5 $wt.\%$ ZnFeO and (b) 5 $wt.\%$ ZnFeO; image showing dislocations in the YBCO matrix.

This micrograph reveals the presence of high density of nano-sized scale inhomogeneities, incorporated within the YBCO matrix. EDS analyses collected from these nanophases show the presence of Zn and Fe and from outside these inhomogeneities exist only the YBCO phase. In fact, Zn-Fe rich inhomogeneities generate high densities of twins and then increase the density of dislocations in the matrix. These defects can contribute to the scattering of the conduction electrons and work as flux pinning centers.

Measurements of the resistivity dependence on the temperature $\rho(T)$ for free and doped samples with various amounts of ZnFeO are shown in Fig. 4. As can be seen from this figure, the samples sintered with $x \leq 7$ show a superconducting transition to zero resistance at T > 20 K, except the case for ZnFeO with $x = 7$. The normal state resistivity of samples sintered with an amount $x \leq 1$ of ZnFeO shows a linear function of temperature.

Multi-Knowledge Electronic Comprehensive Journal For Education And Science Publications (MECSJ)
ISSUE (28), January (2020)
ISSN: 2616-9185
www.mecsj.com

As the additives concentration increased, the normal state resistivity shows a transition from metallic to insulator behavior. Resistivity upturns have been observed for $x \geq 3$ of ZnFeO additions. W. Chen et al. [49] have explained the observed resistivity upturn of cuprates by considering the effects of disorder produced by Zn substitution or electronic irradiation associated with a strong electronic correlation. They find that correlation- induced magnetic droplets around impurities and give rise to an extra scattering which causes the resistivity upturns.

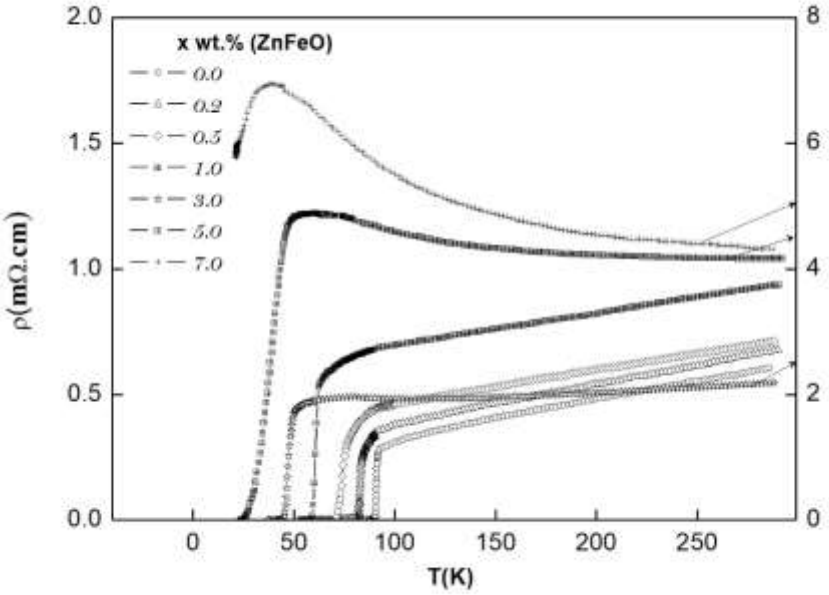

Fig. 4: Resistivity dependences on the temperature for samples sintered with various amounts of ZnFeO nanoparticles.

Fig. 5 shows the variation of the zero-resistance temperature T_{co} and the onset transition temperature T_c^{onset} for YBCO with different amounts of ZnFeO. It can be seen that T_c^{onset} and T_{co} decrease with increasing$x$. Low concentration added nanoparticles leads to a relatively sharp superconducting transition and a broad transition take place for ZnFeO addition greater than1 $wt.\%$. Variations of the T_{co} versus $x\ wt.\%$ have two different regions; a rapid decrease of T_{co} for low concentration (up to $1\ wt.\%$ of ZnFeO) this behavior is attributed to the homogeneity of the samples and/or to the disruption of Cu-O weak links in chain [50 - 53].

A gradual decrease of T_{co} up to $7\ wt.\%$ may be attributed to the formation of Fe-rich phase [52, 53], this result is in agreement with XRD and TEM analysis. Moreover, the superconductivity is more suppressed for ZnFeO addition greater than $1\ wt.\%$ at the rate of 8.3K/at% compared to our previous study with ZnO nanoparticle addition where T_{co} decreases at the rate of 5.3K/at% [41]. S. B. Ogale et al. [32] reported that Fe/Zn dual doped YBCO samples leads to a significantly higher Tc suppression as compared to the cases of separate equivalent total doping of Fe or Zn. It appears that the process of hole doping from chains to the CuO_2 planes is partially obstructed leading to a reduction in the density of holes available in the plans. Others, reported that pair-breaking due to the spin scattering across magnetic nanoparticles dispersed in the inter-grain region of CuTl-1223 matrix may be responsible for the superconductivity suppression [35, 54, 55].

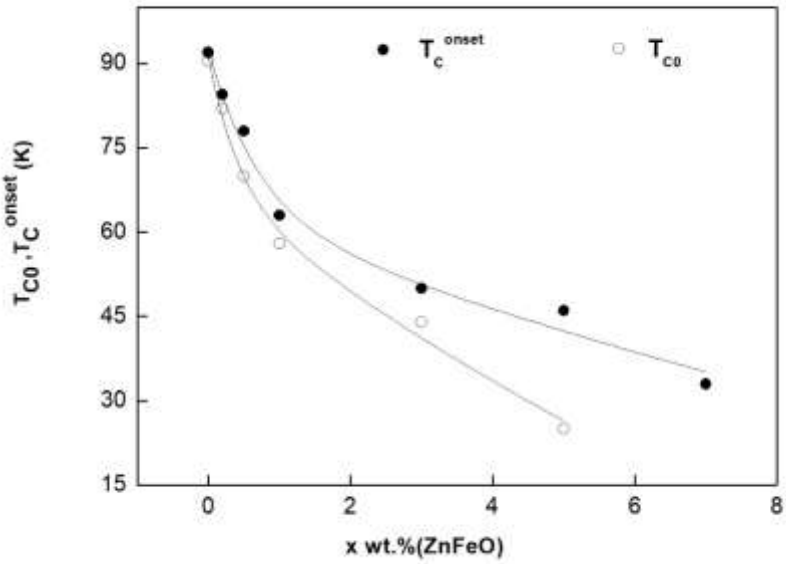

Fig. 5: Zero-resistivity temperature T_{co} and onset transition temperature T_c^{onset} for YBCO with different amounts of ZnFeO. Solid lines are just guides to the eyes.

In other hand, we can observe that the normal state resistivity increases with the addition of ZnFeO nanoparticles. As the normal state resistivity is regarded as the measure of disorder, it shows that the presence of ZnFeO in the matrix increases the amount of disorder.

Multi-Knowledge Electronic Comprehensive Journal For Education And Science Publications (MECSJ)
ISSUE (28), January (2020)
ISSN: 2616-9185
www.mecsj.com

This is evident from Fig. 6 which exhibits a variation of the increase in residual resistivity $\Delta\rho_0$ with the amount x of ZnFeO, where $\Delta\rho_0 = \rho(x) - \rho(0)$, $\rho(x)$ is obtained by fitting a straight line in the linear portion of normal state resistivity of different samples $0 \leq x \leq 7$ from room temperature to 0 K. We note a slowly variation of $\Delta\rho_0$ for $x \leq 1$ then the residual resistivity increases more rapidly as the amount of ZnFeO increases.

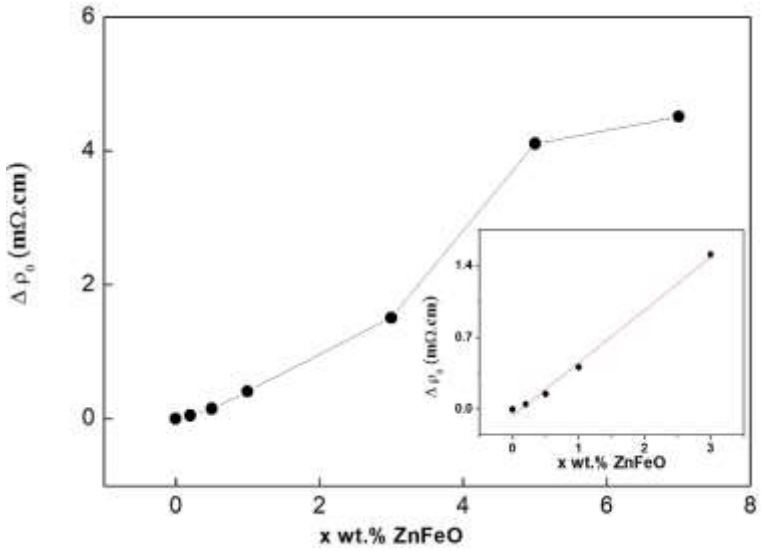

Fig. 6: Evolution of the increase in residual resistivity $\Delta\rho_0$ with $x\ wt.\%$ (ZnFeO). Solid lines are just guides to the eyes. In the inset, the linear relation of $\Delta\rho_0$ with the amount of ZnFeO for $x \leq 3$.

If we assume as is usually done in cuprates, that the contribution of the s-wave impurity scattering follows the formula: $\Delta\rho_0 = 4(h/2\pi e^2)(n_i/n)sin^2\delta_0$ (1)

Where n_i and n are impurity and carrier concentrations respectively, and δ_0 is the scattering phase shift [8]. The fit of the experimental points of $\Delta\rho_0$ with ZnFeO addition show a linear behavior for $x \leq 3$ (see inset fig 6). This result is predicted by the formula (1) as the charge carrier density n is almost unchanged where the oxygen content y is independent of ZnFeO additions and consider the phase shift δ_0 not affected. We may conclude that for low ZnFeO additions the main cause of the residual resistivity is the impurity present in the matrix. For an amount of ZnFeO more than 3 $wt.\%$, the dependence of $\Delta\rho_0$ on x is not only controlled by the greater number of defects and heterogeneities in ZnFeO samples, but the impact of scattering phase shift may have an important role [56].

To more investigate the normal state resistivity $\rho(T)$, the change from a metallic to an insulating behavior allows one to argue that the quantum percolation theory, can interpret both the insulating and the metallic behaviors of different samples either by VRH and CG mechanisms. The temperature dependence of resistivity is described by the relation:

$$\rho(T) = \rho_o \left(\frac{T}{T_o}\right)^{2p} exp\left(\frac{T_o}{T}\right)^{p} \quad (2)$$

Where ρ_o and T_o are constants characterizing a given material and p depends on both the dimensionality of the system and the shape of the density of states (DOS) at the Fermi level. For non-interacting charge carriers, VRH model predicts a value of p $=$ 1/3 in 2D and p $=$ 1/4 in 3D localization [57]. However, when localized carriers interact via the coulomb potential on localized states, a soft gap in the DOS near the Fermi level is created causing new temperature dependence of the hopping conductivity and p $=$ 1/2 in both 2D and 3D [58].

The resistivity data of ZnFeO added samples in the normal state was fitted by equation (2) leaving the exponent value p as variable are shown in Fig. 7 and the fitting parameters are listed in Table 1. We found that the resistivity behaviors of ZnFeO added samples with $x \leq 0.5$ were best fitted with p $= 1/2$ in a wide temperature rang up to 290 K, which corresponds to CG conduction mechanism. Many groups indicated that CG mechanism is well established for low doped HTSC phases [34, 41]. The system is observed to undergo a crossover from CG to 2D-VRH mechanism in the concentration range $0.5 < x \leq 3$ that means probably the hopping occurs in CuO2 planes [59, 60] and from 2D-VRH to 3D-VRH mechanism for $3 < x \leq 7$. Similar results were reported where the three mechanisms occurred at different nanoparticle additions [41, 42]. In other hand, we suggest that the observed 3D hopping conductivity is mainly due to the presence of magnetic atom Fe in ZnO nanoparticle. In Fact, previous study [41] showed that only 2D-VRH mechanism is well established for nano ZnO addition greater than 3 $wt.\%$.

Multi-Knowledge Electronic Comprehensive Journal For Education And Science Publications (MECSJ)
ISSUE (28), January (2020)
ISSN: 2616-9185
www.mecsj.com

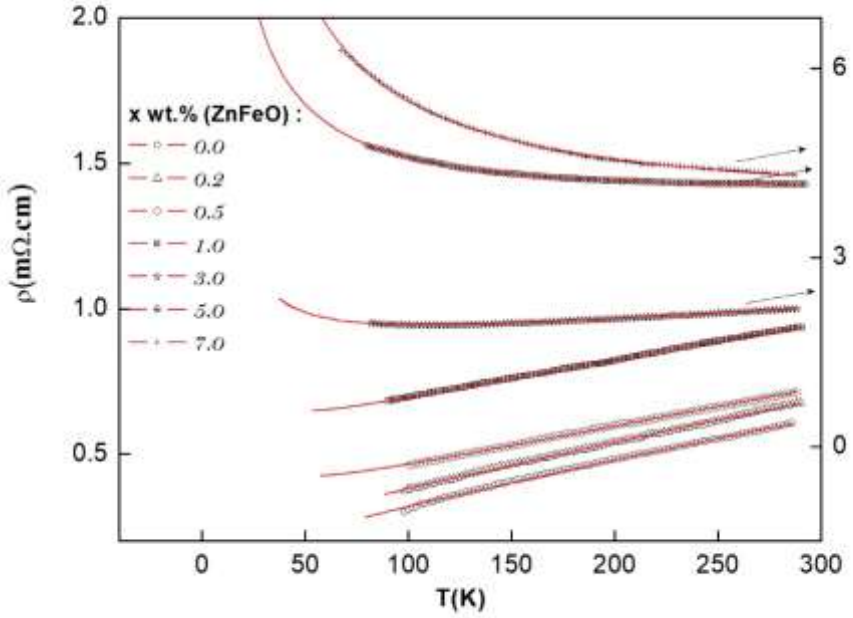

Fig. 7: Fitting data of the resistivity with both the CG and the VRH models for samples sintered with various amounts of ZnFeO nanoparticles.
Lines are VRH and CG fits and symbols are experimental data.

From the fitting parameter T_o (see table 1), we calculate the localization length d which represents the decay length of localized carrier wave function.

Table 1: The fitting parameters ρ_o and T_o of resistivity curves deduced from equation (2) for different amount of ZnFeO

x	ZnFeO		
wt.%	$\rho_o(m\Omega.cm)$	$T_o(K)$	Best fit
0.0	0.10	67	CG
0.2	0.15	117	CG
0.5	0.19	231	CG
1.0	0.35	267	2D-VRH
3.0	1.05	707	2D-VRH
5.0	2.25	4430	3D-VRH
7.0	2.20	9773	3D-VRH

Multi-Knowledge Electronic Comprehensive Journal For Education And Science Publications (MECSJ)
ISSUE (28), January (2020)
ISSN: 2616-9185
www.mecsj.com

Using the Mott parametrization [57], T_o^{3D} is expressed as: $T_o^{3D} = \frac{16}{k_B D(E_F) d^3}$, where $D(E_F)$ is the density of state in the vicinity of the Fermi level and k_B is the Boltzman constant. By using the current estimate of $D(E_F) \approx 10^{21}\ states/eV.cm^3$ in 3D-VRH, the value of d has been estimated. In 2D-VRH, the relation between the fitting parameter T_o^{2D} and the localization length d is given by: $T_o^{2D} = \frac{27}{4\pi k_B D(E_F) d^2}$, where $D(E_F) \approx 10^{14}\ states/eV.cm^2$. However, for the metallic samples, using the CG relation [58], d is given by $d = \frac{e^2}{k_B T_o^{CG} \varepsilon}$, where ε is the dielectric constant usually equal to $\varepsilon = 10$ for the metallic samples [61].

We reported in Fig. 8 the behavior of the localization length d vs doping content of ZnFeO.

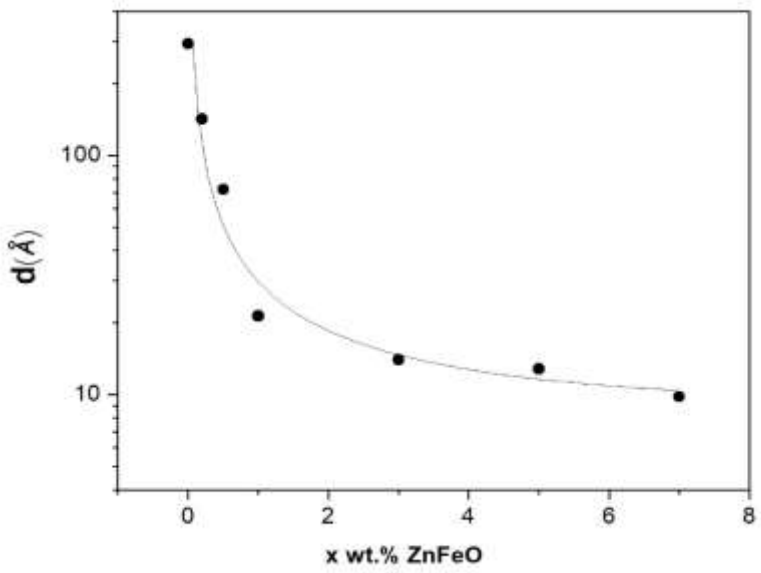

Fig. 8: Localization length d vs doping content of ZnFeO.
Solid lines are just guides to the eyes.

By increasing the doping concentration, the localization length decreases, the hopping range decreases too and the non-added sample ($x = 0$) has the largest distance d. However, the localization length drops quickly for low concentration in ZnFeO system (up to $1\ wt.\%$ of ZnFeO), then the localization length shows a slow decrease for $x \geq 3$ in ZnFeO added samples. For low concentration content ($x < 3$), ZnFeO additions improves the carrier's localization rapidly.

Nevertheless, as the localization length evolves in the same way that the wave-function overlap [62, 63], one may conclude that this overlapping is more effective with ZnFeO addition. This result can be interpreted by disorder effects induced in the structure and may be the presence of magnetic Fe atom in the inhomogeneities which need further investigation to conclude about their character. Moreover, the distribution of ZnFeO in the inter-grain region in the YBCO matrix provide weaker tunneling between superconducting grains and as consequence reduces the pathways for charge carriers leading to the observed localization length behavior [42].

4. Conclusion

The effect of nano-size ZnFeO (30 nm in diameter) addition on the microstructure and the normal state transport properties of polycrystalline YBCO was systematically studied. Samples were synthesized in air using a standard solid-state reaction technique by adding nano-sized particles up to 7.0 $wt.\%$. XRD experiments are performed and the results are refined by the Rietveld method. XRD analysis shows a predominantly single-phase perovskite structure with orthorhombic symmetry. TEM and EDS analyses show the presence of nanometer size inhomogeneities embedded in the superconducting matrix, generate high densities of dislocations in ZnFeO samples. Nano-sized particles addition modifies the electrical behavior from metallic to insulating with increasing ZnFeO concentration leading to increases of residual resistivity. In order to interpret the normal state electrical properties of the samples over a wide range of temperature, the quantum percolation theory based on localized states is applied. The fitting data with variable range hopping model shows a crossover between CG and VRH mechanisms as increasing the ZnFeO concentration. The localization length has been calculated for various x which as expected decreases as the systems approaches the insulating region. The results of the localization length behavior and the suppression of T_{co} can be interpreted by disorder effects induced by nano ZnFeO additions.

References

1- Reiner, M., Gigl, T., Jany, R., Hammerl, G., & Hugenschmidt, C. (2018). Impact of oxygen diffusion on superconductivity in $YBa_2Cu_3O_{7-\delta}$ thin films studied by positron annihilation spectroscopy. *Physical Review B, 97*(14), 144503.

2- Hapipi, N. M., Chen, S. K., Shaari, A. H., Kechik, M. M. A., Tan, K. B., & Lim, K. P. (2018). Superconductivity of Y_2O_3 and $BaZrO_3$ nanoparticles co-added $YBa_2Cu_3O_{7-\delta}$ bulks prepared using co-precipitation method. *Journal of Materials Science: Materials in Electronics, 29*(21), 18684-18692.

3- Li, P., Abraimov, D., Polyanskii, A., Kametani, F., & Larbalestier, D. (2015). Study of grain boundary transparency in $(Yb_{1-x}\ Ca_x)\ Ba_2Cu_3O$ bicrystal thin films over a wide temperature, field, and field orientation range. *Physical Review B, 91*(10), 104504.

4- Achkar, A., Mao, X., McMahon, C., Sutarto, R., He, F., Liang, R., Bonn, D., Hardy,W., & Hawthorn, D. (2014). Impact of quenched oxygen disorder on charge density wave order in $YBa_2Cu_3O_{6+x}$. *Physical review letters, 113*(10), 107002.

5- Uykur, E., Tanaka, K., Masui, T., Miyasaka, S., & Tajima, S. (2014). Persistence of the superconducting condensate far above the critical temperature of $YBa_2(Cu, Zn)_3O_y$ revealed by c-axis optical conductivity measurements for several Zn concentrations and carrier doping levels. *Physical review letters, 112*(12), 127003.

6- Zeng, S., Wang, X., Lü, W., Huang, Z., Motapothula, M., Liu, Z., Zhao, Y., Annadi, A., Dhar, S., Mao, H., Chen, W., Venkatesan, T., & Ariando. (2012). Metallic state in La-doped $YBa_2Cu_3O_y$ thin films with n-type charge carriers. *Physical Review B, 86*(4), 045124.

7- Uchiyama, H., Matsukura, N., & Chikumoto, N. (2010). Carbonate effects in single-crystalline $YBa_2\ Cu_3O_{7-\delta}$. *Physical Review B, 81*(6), 060511.

8- Chien, T., Wang, Z., & Ong, N. P. (1991). Effect of Zn impurities on the normal-state Hall angle in single-crystal $YBa_2Cu_{3-x}Zn_xO_{7-\delta}$. *Physical review letters, 67*(15), 2088.

9- Fukuzumi, Y., Mizuhashi, K., Takenaka, K., & Uchida, S. (1996). Universal superconductor-insulator transition and T_c depression in Zn-substituted high-T_c cuprates in the underdoped regime. *Physical review letters, 76*(4), 684.

10- Uchida, S. (2001). Zn-impurity effects on high-temperature superconductivity. *Physica C: Superconductivity, 357*, 25-29.

11- Le Tacon, M., Sacuto, A., Gallais, Y., Colson, D., & Forget, A. (2007). Investigations of the relationship between T_c and the superconducting gap under magnetic and nonmagnetic impurity substitutions in $YBa_2Cu_3O_{7-\delta}$. *Physical Review B, 76*(14), 144505.

12- Li, P., Zhang, J., Cao, G., Jing, C., & Cao, S. (2004). Suppression of superconductivity by the nonmagnetic ions Zn and Al for the $YBa_2Cu_3O_{7-\delta}$ system: From dopant clusters to carrier localization. Physical Review B, 69(22), 224517.

13- Mellekh, A., Zouaoui, M., Azzouz, F. B., Annabi, M., & Salem, M. B. (2006). Nano-Al_2O_3 particle addition effects on $YBa_2Cu_3O_y$ superconducting properties. *Solid state communications, 140*(6), 318-323.

14- Dadras, S., Liu, Y., Chai, Y., Daadmehr, V., & Kim, K. (2009). Increase of critical current density with doping carbon nano-tubes in $YBa_2Cu_3O_{7-\delta}$. *Physica C: Superconductivity, 469*(1), 55-59.

15- Zhang, H., Liu, Y., Li, H., Qu, J., Li, X., & Feng, Y. (2005). Effects of solid solutions on the superconducting properties of Gd–Ba–Cu–O superconductors. *Superconductor Science and Technology, 18*(10), 1317.

16- Williams, G., Haines, E., & Tallon, J. (1998). Pair breaking in the presence of a normal-state pseudogap in high-T_c cuprates. *Physical Review B, 57*(1), 146.

17- Naqib, S. (2007). The effect of Zn substitution on the suppression of T_c of $Y_{1-x}Ca_xBa_2(Cu_{1-y}Zn_y)_3O_{7-\delta}$ superconductors: the pseudogap and the systematic shift of the optimum hole content. *Superconductor Science and Technology, 20*(10), 964.

18- Williams, G., Tallon, J., & Meinhold, R. (1995). ^{89}Y NMR study of Zn-induced local moments and pair breaking in $Y(Ba_{1-y}La_y)_2(Cu_{1-x}Zn_x)_4O_8$. *Physical Review B, 52*(10), R7034.

19- Markert, J., Dunlap, B., & Maple, M. (1989). Magnetism, Superconductivity, and Chemical Substitutions in $YBa_2Cu_3O_{7-\delta}$. *MRS Bulletin, 14*(1), 37-44.

20- Maeda, H., Koizumi, A., Bamba, N., Takayama-Muromachi, E., Izumi, F., Asano, H., Shimizu, K., Moriwaki, H., Matuyama, H., & Kuroda, Y. (1989). EXAFS and neutron diffraction studies of local and average structures for $YBa_2Cu_{2.8}Zn_{0.2}O_{7-\delta}$. *Physica C: Superconductivity, 157*(3), 483-490.

21- Nachumi, B., Keren, A., Kojima, K., Larkin, M., Luke, G., Merrin, J., Tchernyshöv, O., Uemura, Y., Ichikawa, N., Goto, M., & Uchida, S. (1996). Muon spin relaxation studies of Zn-substitution effects in high-T_c cuprate superconductors. *Physical review letters, 77*(27), 5421.

22- Matsunaka, D., Kasai, H., Diño, W. A., & Nakanishi, H. (2003). Magnetic properties in the high-temperature cuprate superconductors with nonmagnetic impurities. *Physical Review B, 68*(5), 054503.

23- Savinkov, A., Dooglav, A., Alloul, H., Mendels, P., Bobroff, J., Collin, G., & Blanchard, N. (2009). Dynamics and distribution of doped holes in the CuO_2 plane of slightly doped $Y_{1-y}Ca_yBa_2Cu_3O_6$ studied by Cu(1) NQR. *Physical Review B, 79*(1), 014513.

24- Dallacasa, V., & Feduzi, R. (1995). High-T_c superconductivity in a correlated disorder-induced localized system. *Physica C: Superconductivity*, *251*(1-2), 156-164.

25- Lobo, R., Sherman, E. Y., Racah, D., Dagan, Y., & Bontemps, N. (2002). Localization by disorder in the infrared conductivity of $Y_{1-x}Pr_xBa_2Cu_3O_7$ films. *Physical Review B, 65*(10), 104509.

26- Zagoulaev, S., Monod, P., & Jegoudez, J. (1995). Magnetic and transport properties of Zn-doped $YBa_2Cu_3O_7$ in the normal state. *Physical Review B, 52*(14), 10474.

27- Alloul, H., Mendels, P., Casalta, H., Marucco, J., & Arabski, J. (1991). Correlations between magnetic and superconducting properties of Zn-substituted $YBa_2Cu_3O_{6+x}$. *Physical Review Letters, 67* (1991) 3140.

28- Bridges, F., Boyce, J., Claeson, T., Geballe, T., & Tarascon, J. (1989). Distorted chain sites for Co-and Fe-substituted $YBa_2Cu_3O_{7-\delta}$. *Physical Review B, 39*(16), 11603.

29- Tarascon, J., Barboux, P., Miceli, P., Greene, L., Hull, G., Eibschutz, M., & Sunshine, S. (1988). Structural and physical properties of the metal (M) substituted $YBa_2Cu_{3-x}M_xO_{7-y}$ perovskite. *Physical Review B, 37*(13), 7458.

30- Raffo, L., Licci, F., & Migliori, A. (1994). Copper substitution effects on YBCO microstructure: oxygen ordering, structural coherence and superconductivity. *Physica C: Superconductivity, 235*, 1259-1260.

31- Green, L., & Bagley, B. (1990). Physical Properties of High Temperature Superconductors, vol. II, D. M. Grinsberg, ed., World Scientific, 510-559.

32- Ogale, S., Gapchup, K., Lele, P., Choughule, D., Chikate, R., & Marest, G. (1996). Search for the origin of giant Tc suppression in $YBa_2Cu_3O_{7-\delta}$ doped simultaneously with Fe and Zn. *Physica C: Superconductivity and its applications*, *257*(3-4), 375-381.

33- Mokhtari, Z., Khosroabadi, H., & Akhavan, M. (2004). Thermally activated phase slip and variable range hopping in Tm $(Ba_{2-x}Pr_x)Cu_3O_{7+\delta}$. *physica status solidi (c), 1*(7), 1891-1894.

34- Awad, R., Roumié, M., Abou-Aly, A., Mahmoud, S., & Barakat, M. (2012). Ion Beam Analysis and Normal-State Conduction Mechanisms for (Bi, Pb)-2223 and (Tl, Pb)/Sr-1212 Superconducting Phases Substituted by Ruthenium. *Journal of superconductivity and novel magnetism, 25*(2), 273-291.

35- Mumtaz, M., Baig, M. H., Waqee-ur-Rehman, M., & Khan, M. N. (2018). Magneto-transport properties of Co_3O_4 nanoparticles added $(Cu_{0.5}Tl_{0.5})Ba_2Ca_2Cu_3O_{10-\delta}$ superconducting phase. *Physica B: Condensed Matter, 537*, 283-289.

36- Slimani, Y., Almessiere, M., Hannachi, E., Baykal, A., Manikandan, A., Mumtaz, M., & Azzouz, F. B. (2019). Influence of WO_3 nanowires on structural, morphological and flux pinning ability of $YBa_2Cu_3O_y$ superconductor. *Ceramics International, 45*(2), 2621-2628.

37- Mumtaz, M., Waqee-ur-Rehman, M., & Rabbani, M. (2017). Comparative study of ferromagnetic and anti-ferromagnetic nanoparticles as artificial flux pinning centers in CuTl-1223 superconductor. *Ceramics International, 43*(17), 15842-15845.

38- Zouaoui, M., Ghattas, A., Annabi, M., Azzouz, F. B., & Salem, M. B. (2008). Effect of nano-size ZrO_2 addition on the flux pinning properties of (Bi, Pb)-2223 superconductor. *Superconductor Science and Technology, 21*(12), 125005.

39- Annabi, M., M'chirgui, A., Azzouz, F. B., Zouaoui, M., & Salem, M. B. (2004). Addition of nanometer Al_2O_3 during the final processing of (Bi, Pb)-2223 superconductors. *Physica C: Superconductivity, 405*(1), 25-33.

40- Annabi, M., Bouchoucha, I., Azzouz, F. B., & Salem, M. B. (2010). Effect of ZnO and $Zn_{0,95}Mn_{0,05}O$ nano-particle inclusions on YBCO polycrystalline pinning properties. *IOP Conference Series: Materials Science and Engineering, (13)*, 012009.

41- Bouchoucha, I., Azzouz, F. B., Annabi, M., Zouaoui, M., & Salem, M. B. (2010). The study on the ZnO and $Zn_{0.95}Mn_{0.05}O$ added YBCO system: Investigation of microstructure and transport properties. *Physica C: Superconductivity, 470*(4), 262-268.

42- Salem, M. B., Hamrita, A., Hannachi, E., Slimani, Y., Salem, M. B., & Azzouz, F. B. (2014). The study on SiO_2 nanoparticles and nanowires added YBCuO: Microstructure and normal state electrical properties. *Physica C: Superconductivity, 498*, 38-44.

43- Giri, R., Awana, V., Singh, H., Tiwari, R., Srivastava, O., Gupta, A., Kumaraswamy, B., & Kishan, H. (2005). Effect of Ca doping for Y on structural/microstructural and superconducting properties of $YBa_2Cu_3O_{7-\delta}$. *Physica C: Superconductivity and its applications*, *419*(3-4), 101-108.

44- Waqee-ur-Rehman, M., Qasim, I., Mumtaz, M., Nadeem, K., & Qamar, S. (2016). Resistive transition and flux flow mechanism in CoFe2O4 nanoparticles added $Cu_{0.5}Tl_{0.5}Ba_2Ca_2Cu_3O_{10-\delta}$ superconductor. *Journal of Alloys and Compounds*, *657*, 348-352.

45- Salem, M. B., Almessiere, M., Al-Otaibi, A., Salem, M. B., & Azzouz, F. B. (2016). Effect of SiO_2 nanoparticles and nano-wires on microstructure and pinning properties of $YBa_2Cu_3O_{7-\delta}$. *Journal of Alloys and Compounds*, *657*, 286-295.

46- Benzi, P., Bottizzo, E., & Rizzi, N. (2004). Oxygen determination from cell dimensions in YBCO superconductors. *Journal of Crystal Growth*, *269*(2-4), 625-629.

47- Zhang, Y., Hu, S., Wang, D., Liu, Y., & Li, P. (2010). Superconductivity without relation to valence electrons in (Fe, Zn) doped YBCO systems. *Journal of Low Temperature Physics*, *160*(1-2), 49-57.

48- Zhang, H., Zhao, X., Zhao, Y., Liu, S., & Zhang, Q. (1989). Oxygen content is not the predominant factor for high Tc superconductivity in Y-Ba-Cu-O system. *Solid state communications*, *72*(1), 75-79.

49- Chen, W., Andersen, B. M., & Hirschfeld, P. (2009). Theory of resistivity upturns in metallic cuprates. *Physical Review B*, *80*(13), 134518.

50- Clark, G., Marwick, A., Koch, R., & Laibowitz, R. (1987). Effects of radiation damage in ion-implanted thin films of metal-oxide superconductors. *Applied Physics Letters*, *51*(2), 139-141.

51- Li, Y., Linzen, S., Machalet, F., Schmidl, F., & Seidel, P. (1995). Recovery of superconductivity and recrystallization of ion-damaged $YBa_2Cu_3O_{7-x}$ films after thermal annealing treatment. *Physica C: Superconductivity*, *243*(3-4), 294-302.

52- Wu, X., Tan, W., Xu, Y., Zhang, E., Du, J., Hu, A., Jiang, S., & Gao, J. (2003). Structure and spin-gap in the normal state of $Y_{1-x}Ca_xBa_{1.9}Nd_{0.1}Cu_3O_y$ cuprates. *Physica C: Superconductivity*, *398*(3-4), 131-140.

53- Nikogosyan, S., Sahakyan, A., Yeritsyan, H., Grigoryan, V., Zargaryan, E., & Sarkissyan, A. (1998). Superconducting properties of $YBa_2Cu_{3-x}Fe_xO_y$ ceramics with small x. *Physica C: Superconductivity*, *299*(1-2), 65-70.

54- Qasim, I., Waqee-ur-Rehman, M., Mumtaz, M., & Nadeem, K. (2016). Role of Co nanoparticles in CuTl-1223 superconductor. *Ceramics International*, *42*(1), 1122-1127.

55- Qasim, I., Waqee-ur-Rehman, M., Mumtaz, M., Hussain, G., Nadeem, K., & Shehzad, K. (2016). Ferromagnetic (Ni) nanoparticles–CuTl-1223 superconductor composites. *Journal of Magnetism and Magnetic Materials*, *403*, 60-67.

56- Jamadar, T., Roy, A., & Ghosh, A. K. (2013). Suppression of critical temperature and charge localization in underdoped $NdBa_2Cu_{3-x}Zn_xO_{7-y}$. *Physica C: Superconductivity*, *492*, 59-63.

57- Mott, N., & Davis, E. (1979). Electronic processes in non-crystalline materials, 2nd edn. Clarendon. In: Oxford.

58- Efros, A., & Shklovskii, B. I. (1975). Coulomb gap and low temperature conductivity of disordered systems. *Journal of Physics C: Solid State Physics*, *8*(4), L49.

59- Mofakham, S., Mazaheri, M., & Akhavan, M. (2008). Two-dimensional mechanism of electrical conductivity in $Gd_{1-x}Ce_xBa_2Cu_3O_{7-\delta}$. *Journal of Physics: Condensed Matter*, *20*(34), 345221.

60- Mohammadizadeh, M., & Akhavan, M. (2003). Normal state conduction in $Gd(Ba_{2-x}Pr_x)Cu_3O_{7+\delta}$. *The European Physical Journal B-Condensed Matter and Complex Systems*, *33*(4), 381-390.

61- Quitmann, C., Fleuster, M., Jarchow, C., Andrich, D., Paulose, P., & Güntherodt, G. (1991). Electronic transport across the superconductor-insulator transition in $Bi_2Sr_2[Ca_{1-x}(Y,Ce)_x]Cu_2O_{8+y}$. *Physica C: Superconductivity*, *185*, 1337-1338.

62- Quitmann, C., Andrich, D., Jarchow, C., Fleuster, M., Beschoten, B., Güntherodt, G., Moshchalkov, V., Mante, G., & Manzke, R. (1992). Scaling behavior at the insulator-metal transition in $Bi_2Sr_2(Ca_z\ R_{1-z})Cu_2O_{8+y}$ where R is a rare-earth element. *Physical Review B*, *46*(18), 11813.

63- Beschoten, B., Sadewasser, S., Güntherodt, G., & Quitmann, C. (1996). Coexistence of superconductivity and localization in $Bi_2Sr_2(Ca_z, Pr_{1-z})Cu_2O_{8+y}$. *Physical review letters*, *77*(9), 1837.